ACS OMEGA

http://pubs.acs.org/journal/acsodf
Article

Significant Increase in the Dipole Moment of Graphene on Functionalization: DFT Calculations and Molecular Dynamics Simulations

Madhur Babu Singh, Pallavi Jain, Faruq Mohammad, Prashant Singh,* Indra Bahadur, and Oyirwoth P. Abedigamba*

Cite This: *ACS Omega* 2024, 9, 16458−16468
Read Online

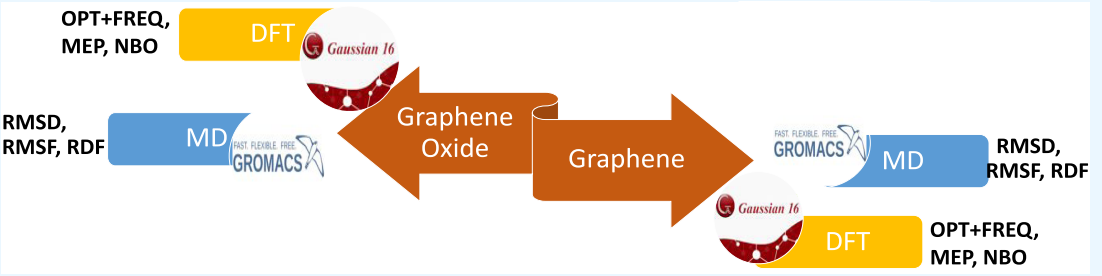

ABSTRACT: The limited solubility of graphene in water can be attributed to the existence of $\pi-\pi$ bonds connecting its layers. Functionalized graphene or graphene oxide (GO) is frequently produced in order to overcome the shortcomings of graphene. Using density functional theory (DFT) calculation, functionalized graphene with various combinations of hydroxyl, epoxy, and carboxylic functional groups were investigated computationally. The study focused on the effects of functional group combinations on the highest occupied molecular orbital (HOMO) and lowest unoccupied molecular orbital (LUMO) energies, giving information about the chemical reactivity and stability of the molecules under investigation. Global chemical reactivity descriptors, including chemical hardness, softness, electronegativity, chemical potential, and electrophilicity index, were calculated to further elucidate the overall stability and reactivity of the molecules. The results demonstrated that the introduction of oxygen-containing functional groups on graphene significantly influenced its electronic properties, leading to variations in the chemical reactivity and stability. Molecular electrostatic potential (MEP) maps highlighted the susceptibility of specific regions to electrophilic and nucleophilic attacks. The flexibility and stability of functionalized graphene through root mean square fluctuation (RMSF) and root mean square deviation (RMSD) analyses indicate the stability of functionalized graphene in water. This comprehensive computational investigation provides valuable insights into the design and understanding of functionalized graphene for potential applications in drug delivery.

1. INTRODUCTION

Two-dimensional (2D) materials have become the subject of intense scientific investigation due to the unique properties and phenomena they exhibit that are not present in bulk materials. Primarily among these substances is graphene, which is obtained from graphite and consists of a solitary monolayer of carbon atoms organized in a hexagonal lattice. Graphene demonstrates exceptional mechanical, electrical, optical, thermal, and catalytic characteristics, along with its nanoscale super-hydrophobicity.[1,2]

The restricted solubility of graphene in water is due to the presence of $\pi-\pi$ bond between the layers.[3] The $\pi-\pi$ interactions between adjacent graphene layers play a crucial role in determining the solubility of graphene. These interactions arise from the overlapping π orbitals of carbon atoms in the hexagonal lattice structure of graphene. When multiple graphene layers stack together, these π orbitals align and form $\pi-\pi$ bonds, which contribute to the structural stability of graphene but also pose challenges to its solubility in various solvents.[4] Therefore, graphene oxide (GO) frequently comes into existence as it overcomes the limitations of graphene. The hydrophilic nature and water dispersibility of GO are due to the presence of polar functional groups and it important for facilitating the processing and chemical modification of GO.[5] The oxidation process introduces oxygen-containing functional groups, such as epoxides, hydroxyls, and carboxyls, onto the graphene lattice. These functional groups disrupt the $\pi-\pi$ interactions between

Received: January 5, 2024
Revised: February 23, 2024
Accepted: February 28, 2024
Published: March 26, 2024

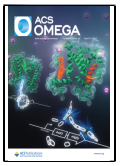

https://doi.org/10.1021/acsomega.4c00173
ACS Omega 2024, 9, 16458−16468

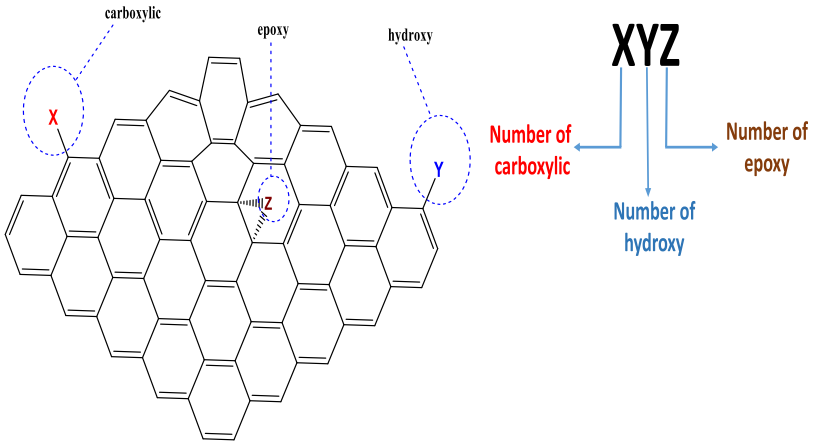

Figure 1. Representation of functional groups on graphene.

graphene layers by introducing steric hindrance and electrostatic repulsion forces. As a result, the interlayer spacing increases and the graphene sheets become more hydrophilic due to the presence of polar functional groups. The introduction of oxygen functional groups not only enhances the solubility of graphene oxide but also imparts additional functionalities and properties to the material.[6] The hydrophilic nature of GO allows it to readily disperse in aqueous solvents, making it compatible with a wide range of biological and environmental applications. Furthermore, the presence of functional groups enables facile chemical modification and functionalization of GO, expanding its utility in areas such as sensors, catalysis, energy storage, and biomedical applications.[7] This attribute is significant for improving the material's compatibility with water-based surroundings.[8]

The properties and applications of functionalized graphene including GO are closely intertwined with its structural configuration and composition, owing to its heterogeneous nature.[9−11] The utilization of these exceptional characteristics has led to a growing fascination with GO as an important material for the progression of electronic devices, drug delivery, and water purification.[12,13] GO is distinguished by its single-atom-thick carbon layers in sp^3 structure, decorated with hydroxyl, carbonyl, carboxyl, and epoxy groups and it has been effective in a various of applications.[14,15] Notwithstanding the substantial amount of attention that GO has garnered, obstacles continue to impede its complete realization.[16] The potential applications of graphene in nanoelectronics are constrained by its zero band gap, which has led to the investigation of derivatives like GO.[17−19] However, the ongoing debate surrounding the composition and intricate structure of GO serves to underscore the material's complexity.[20]

Hydrophilic moieties are characterized by the presence of hydroxyl and epoxide groups along the basal plane and carboxyl groups along the periphery. The aim of this research work is to understand the computational investigation into the electronic properties of functionalized graphene on the functional groups in different combinations. Herein, the hydroxyl, epoxy, and carboxylic groups are varied to manipulate the physical and chemical properties of functionalized graphene.

2. COMPUTATIONAL DETAILS

2.1. DFT Calculation. DFT were performed to investigate the characteristics of graphene, and functionalized graphene containing different functional groups in combinations. Structures of all functionalized graphene and graphene were designed using ChemDraw 15,[21] and the representation of function is shown in Figure 1. All DFT calculations were performed using the Gaussian 16 software package, and the visualization of the result was done by GaussView 06.[22,23] The B3LYP hybrid functional, known for its precise description of molecular structures and energetics, was selected as the exchange-correlation functional. This functional integrates the Becke three-parameter exchange (B3) with the Lee−Yang−Parr correlation (LYP), resulting in a well-balanced approach to accounting for both short- and long-range correlation effects.[24,25] The 6-311 + G(d,p) basis set was used to represent the arrangement of carbon, oxygen, and hydrogen atoms in graphene and functionalized graphene.[26] This basis set achieves a satisfactory balance between computing efficiency and accuracy in accurately representing the electrical structure of the system. Geometry optimizations and frequency calculations were performed using the same level of theory to guarantee convergence to the structure with the lowest energy.[27,28] In order to examine the effect of various functional group coverages on functionalized graphene, many models were created by systematically altering the quantities of hydroxy, epoxy, and carboxylic groups. The models were fine-tuned until the forces exerted on the atoms reached a level below 0.0001 Hartree−Bohr and remained stable.

2.2. Molecular Dynamics (MD) Simulations. GROMACS was used for all simulations, using the CHARMM36 force field for all compositions.[29,30] Ligand was first optimized with Gaussian, and then its topology was prepared by using the online web server swissParam (https://old.swissparam.ch/). The leapfrog method was used to integrate Newton's equations of motion. The ligand was immersed in a cubic box applying the transferable intermolecular potential together with a TIP3P water model.[31] The use of periodic boundary conditions allowed for the neutralization of the ligand by the use of Monte Carlo ion placing with Na^+ and Cl^- ions.[32] The MD simulations consisted of three steps: an initial optimization stage lasting 10 ps, followed by two equilibration stages for 100 ps each, performed under the NVT and NPT settings.[33] The MD simulations, running for 500 ns, used the Particle Mesh Ewald method to handle long-range electrostatic interactions.

https://doi.org/10.1021/acsomega.4c00173
ACS Omega 2024, 9, 16458−16468

Table 1. Different Physiochemical Descriptors of Graphene and Functionalized Graphene

	HOMO	LUMO	H − L	L + H	η	χ	S	μ	ω
001	−0.16314	−0.13571	−0.02743	−0.29885	0.013715	0.149425	36.456435	−0.149425	0.8139931
002	−0.17343	−0.13279	−0.04064	−0.30622	0.02032	0.15311	24.606299	−0.15311	0.5768374
003	−0.17817	−0.13186	−0.04631	−0.31003	0.023155	0.155015	21.593608	−0.155015	0.5188869
010	−0.15553	−0.13213	−0.0234	−0.28766	0.0117	0.14383	42.735043	−0.14383	0.8840628
020	−0.15593	−0.13249	−0.02344	−0.28842	0.01172	0.14421	42.662116	−0.14421	0.8872237
030	−0.1533	−0.13022	−0.02308	−0.28352	0.01154	0.14176	43.327556	−0.14176	0.8707061
100	−0.16729	−0.14368	−0.02361	−0.31097	0.011805	0.155485	42.354934	−0.155485	1.0239553
200	−0.1678	−0.14464	−0.02316	−0.31244	0.01158	0.15622	43.177893	−0.15622	1.053743
210	−0.16312	−0.14033	−0.02279	−0.30345	0.011395	0.151725	43.878894	−0.151725	1.010113
211	−0.16126	−0.13639	−0.02487	−0.29765	0.012435	0.148825	40.209087	−0.148825	0.8905863
220	−0.16036	−0.13904	−0.02132	−0.2994	0.01066	0.1497	46.904315	−0.1497	1.0511299
221	−0.16159	−0.1369	−0.02469	−0.29849	0.012345	0.149245	40.502228	−0.149245	0.9021495
222	−0.16311	−0.13728	−0.02583	−0.30039	0.012915	0.150195	38.714673	−0.150195	0.8733464
300	−0.17363	−0.1522	−0.02143	−0.32583	0.010715	0.162915	46.663556	−0.162915	1.2385113
310	−0.16908	−0.14758	−0.0215	−0.31666	0.01075	0.15833	46.511628	−0.15833	1.1659716
311	−0.17055	−0.14642	−0.02413	−0.31697	0.012065	0.158485	41.442188	−0.158485	1.040924
320	−0.16911	−0.14719	−0.02192	−0.3163	0.01096	0.15815	45.620438	−0.15815	1.141032
321	−0.16892	−0.14795	−0.02097	−0.31687	0.010485	0.158435	47.687172	−0.158435	1.1970267
322	−0.17183	−0.15066	−0.02117	−0.32249	0.010585	0.161245	47.236656	−0.161245	1.2281507
330	−0.16912	−0.14709	−0.02203	−0.31621	0.011015	0.158105	45.392646	−0.158105	1.1346887
331	−0.17069	−0.14949	−0.0212	−0.32018	0.0106	0.16009	47.169811	−0.16009	1.208906
332	−0.17182	−0.14996	−0.02186	−0.32178	0.01093	0.16089	45.745654	−0.16089	1.1841533
333	−0.17203	−0.14961	−0.02242	−0.32164	0.01121	0.16082	44.603033	−0.16082	1.1535715
graphene	−0.15914	−0.13437	−0.02477	−0.29351	0.012385	0.146755	40.371417	−0.146755	0.8694804

This technique was chosen to maintain the stability of the ligand.[34] The CHARMM36m force field was used to simulate the behavior of ions, while GROMACS was employed to examine MD trajectories for comparison data, such as root mean square deviation (RMSD), radial distribution function (RDF) and root mean square fluctuation (RMSF).[35]

3. RESULTS AND DISCUSSION

3.1. Analysis of Information Obtained from DFT Computations. In this study, the electron-donating and -receiving abilities of the graphene and functionalized graphene were assessed through the determination of the highest occupied molecular orbital (HOMO) and lowest unoccupied molecular orbital (LUMO) energies. These molecular orbitals play a pivotal role in elucidating the electronic properties, chemical reactivity, and pharmaceutical aspects while also providing insights into biological mechanisms. The energy gap between these orbitals, referred to as the frontier molecular orbital (FMO) energy gap ($E_{HOMO} - E_{LUMO}$), was determined and given in Table 1. This energy gap serves as a key indicator of the stability of the molecular structure. A smaller FMO energy gap signifies higher chemical reactivity, biological activity, and polarizability of the studied molecule. The graphical representation of the FMO's distribution of the compound is presented in Figure 2, providing a visual depiction of the electron density distribution in the HOMO and LUMO orbitals. On increasing the number of epoxy groups (001−003) on a graphene sheet, there is an observed rise in the $E_{HOMO} - E_{LUMO}$ energy gap (0.02743 to 0.04631 hartree/particle). This indicates a gain in stability and a reduction in the chemical reactivity of the graphene sheet with an increasing number of epoxy groups. No notable change in the $E_{HOMO} - E_{LUMO}$ energy gap is seen when the number of hydroxy groups is increased in hydroxy functionalized graphene (010−030). The $E_{HOMO} - E_{LUMO}$ energy gap of carboxyl functionalized graphene (100−300) decreases as the number of carboxyl groups increases, indicating an increase in chemical reactivity. The $E_{HOMO} - E_{LUMO}$ energy gap of 210, 211, 220, 221, and 222 with a fixed number of carboxylic acid two and varying numbers of epoxy and hydroxy groups are 0.02279, 0.02487, 0.02132, 0.02469, and 0.02583 hartree/particle, respectively, indicating that there is no significant change in energy. The $E_{HOMO} - E_{LUMO}$ energy gaps of 310, 311, 320, 321, 322, 330, 331, 332, 333, and graphene are 0.0215, 0.02413, 0.02192, 0.02097, 0.02117, 0.02203, 0.0212, 0.02186, 0.02242, and 0.02477 hartree per particle, respectively. Out of all of the functionalized graphene, 321 and 322 had the smallest $E_{HOMO} - E_{LUMO}$ energy gap of 0.02097 and 0.02117 hartree/particle, respectively. This indicates that they exhibit greater chemical reactivity, biological activity, and polarizability.

Global chemical reactivity descriptors are commonly employed to elucidate the overall stability of molecules in relation to their chemical resilience, offering insights into molecular reactivity.[36] Various global chemical reactivity descriptors were calculated, such as E_{HOMO}, E_{LUMO}, the $E_{HOMO} - E_{LUMO}$ energy gap, hardness (η), softness (S), electronegativity (χ), chemical potential (μ), and electrophilicity index (ω). The calculated chemical hardness, chemical potential, electrophilicity index, and chemical softness for the studied molecule are given in Table 1.

The chemical potential (μ) defines the tendency of electrons to leave a stable system. A negative chemical potential indicates the stability of a compound, implying that it does not undergo spontaneous decomposition into its constituent atoms. It is observed that the introduction of an oxygen-containing functional group on graphene μ becomes more negative, and 322 with the most negative μ (−0.161245) shows that it is most stable. In chemistry, hardness (η) refers to the ability of a molecule to resist changes in the electron distribution. The

https://doi.org/10.1021/acsomega.4c00173
ACS Omega 2024, 9, 16458−16468

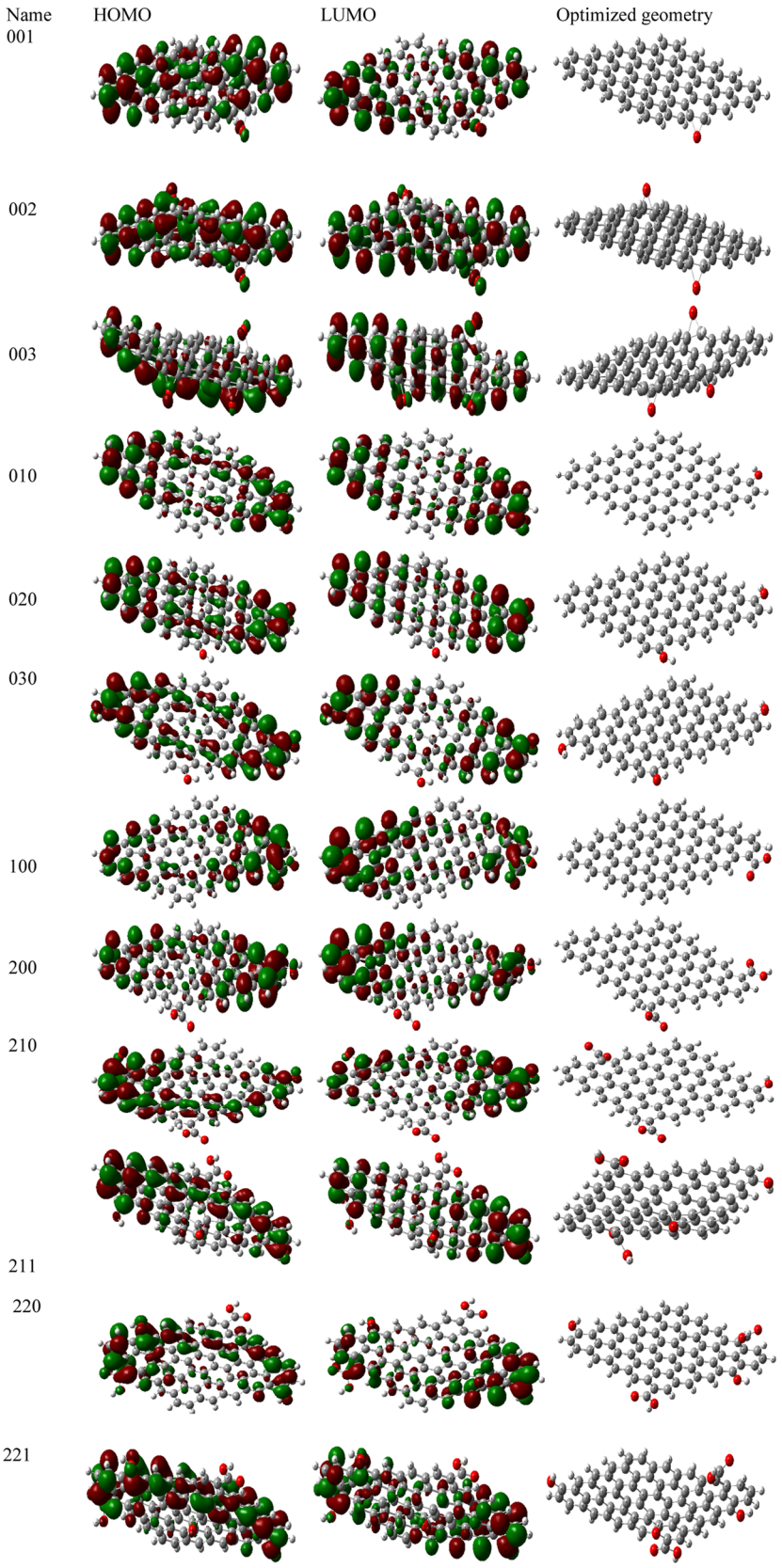

Figure 2. continued

https://doi.org/10.1021/acsomega.4c00173
ACS Omega 2024, 9, 16458−16468

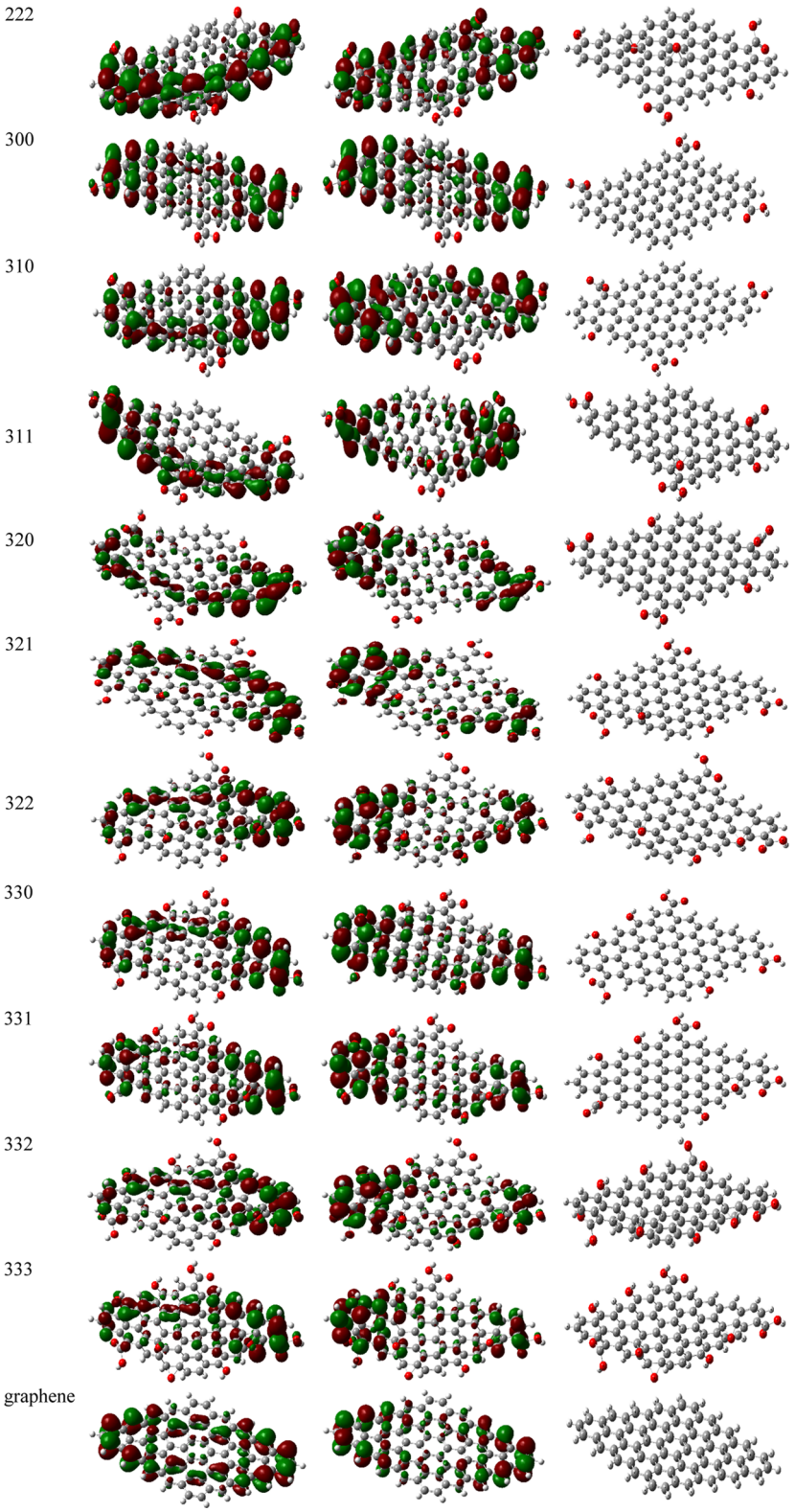

Figure 2. HOMO, LUMO, and optimized geometry of graphene and functionalized graphene.

statement describes the capacity of a chemical system to resist changes in its electron cloud upon exposure to small disturbances during chemical reactions. The $E_{HOMO} - E_{LUMO}$ gap serves as an indication of the molecule's hardness. A significant gap signifies a hard molecule, whereas a small gap indicates a soft molecule that is more prone to reactivity. From all of the designed functionalized graphene, 003 has a maximum η (0.023155).

Softness (S) is the inverse of η and offers an alternative viewpoint on the electron distribution properties of a molecule. The electrophilicity index (ω) is a significant quantum chemical descriptor that plays a critical role in evaluating the toxicity of compounds by determining their reactivity and site

https://doi.org/10.1021/acsomega.4c00173
ACS Omega 2024, 9, 16458−16468

Table 2. Different Thermodynamic Parameters of Graphene and Functionalized Graphene

compound	optimization energy (hartree/particle)	sum of electronic and zero-point energies (hartree/particle)	sum of electronic and thermal energies (hartree/particle)	sum of electronic and thermal enthalpies (hartree/particle)	sum of electronic and thermal free energies (hartree/particle)	dipole moment (Debye)
001	−2756.128462	−2755.447703	−2755.408530	−2755.407585	−2755.512143	7.87
002	−2831.255096	−2830.569842	−2830.530067	−2830.529122	−2830.634786	3.01
003	−2908.380476	−2905.691070	−2905.650637	−2905.649693	−2905.756444	5.02
010	−2756.196671	−2755.516030	−2755.476602	−2755.475658	−2755.580692	7.03
020	−28631.413195	−2830.729065	−2830.688156	−2830.687212	−2830.795288	7.03
030	−2906.631435	−2905.944047	−2905.901645	−2905.900700	−2906.011832	2.23
100	−2869.53099	−2868.848484	−2868.807325	−2868.806381	−2868.915971	27.77
200	−3658.101092	−3057.396887	−3057.352556	−3057.351612	−3057.468882	29.29
210	−3133.30494	−3132.597034	−3132.551454	−3132.550509	−3132.669834	24.46
211	−3209.259500	−3208.550535	−3208.503603	−3208.502659	−3208.625597	20.13
220	−3208.534552	−3207.822378	−3207.775363	−3207.774419	−3207.897751	17.70
221	−3283.650686	−3282.934997	−3282.887169	−3282.886225	−3283.011184	11.31
222	−3358.797434	−3358.077128	−3358.028566	−3358.027621	−3358.153838	2.60
300	3246.663296	−3245.945404	−3245.897969	−3245.897025	−3246.022318	6.05
310	−3321.882045	−3321.159479	−3321.110956	−3321.110012	−3321.236959	20.01
311	−3396.998236	−3396.271485	−3396.222301	−3396.221356	−3396.349814	20.16
320	−3397.099918	−3396.374458	−3396.324287	−3396.323343	−3396.454194	20.33
321	−3472.20042	−3471.470896	−3471.420148	−3471.419204	−3471.551107	20.30
322	−3547.307091	−3546.573663	−3546.522376	−3546.521432	−3546.653023	30.31
330	3472.318315	−3471.588360	−3471.537633	−3471.536689	−3471.667971	19.43
331	−3547.434409	−3546.699939	−3546.648108	−3546.647164	−3546.780798	27.68
332	−3622.524047	−3621.787287	−3621.734598	−3621.733653	−3621.868085	26.88
333	−3697.686542	−3696.945254	−3696.891779	−3696.890835	−3697.027853	27.67
Graphene	−2681.631344	−2680.957005	−2680.918637	−2680.917693	−2681.020886	0.00023

selectivity.[17] The electrophilicity index measures the decrease in energy that occurs when there is a maximum electron transfer between a donor and an acceptor. Essentially, it offers a thorough understanding of the biological effects of the drug−receptor interactions, providing a quantitative assessment of the reactivity and stability of molecules. A higher ω suggests a greater binding capacity, indicating that the molecule can act as an electrophilic species. When there is only the hydroxy or epoxy group present on the graphene sheet, there is a decrease in the value of ω, but when the carboxylic group is introduced on graphene, the value of ω increases. 322 and 300 have the maximum values for ω of 1.2281507 and 1.2385113, respectively. Electronegativity (χ) refers to the ability of molecules to attract electrons, showing their strength to influence the distribution of electrons within a structure. When an oxygen-containing functional group is introduced on graphene, χ increases in comparison to graphene; 322 and 300 have higher values of χ, that is, 0.161245 and 0.162915, respectively.

Initially, the analysis focused on the individual epoxy group, hydroxyl group, and carboxyl group on a 5 × 5 graphene supercell. Subsequently, a graphene sheet containing these functional groups was subjected to DFT calculation, and the thermodynamic parameter of it is given in Table 2. Upon the introduction of oxygen-containing functional groups onto graphene, several key global chemical reactivity descriptors generally exhibit an increase. The hardness of graphene derivatives typically rises due to the electronegative nature of oxygen atoms, which strengthen the carbon−carbon bonds by drawing electron density away from the graphene lattice. Softness increases as the system becomes more flexible, allowing for easier electron density rearrangements. Electronegativity also tends to rise with the presence of oxygen atoms, enhancing the system's ability to attract electrons and participate in chemical reactions. The chemical potential of graphene derivatives increases, reflecting a higher energy state driven by interactions with oxygen atoms. Finally, the electrophilicity index typically increases, indicating an increased propensity for electron acceptance and involvement in electrophilic reactions. These changes in global chemical reactivity descriptors highlight the significant impact of oxygen functionalization on the properties and potential applications of graphene derivatives across various fields.

The optimization energy became more negative, and the dipole moment decreased as the number of epoxy groups on the graphene sheet increased from 1 to 3. The optimization energy becomes more negative and the dipole moment decreases as the number of individual hydroxy and carboxyl groups increases on graphene. When there are two carboxyl and one hydroxy groups on graphene, the dipole moment is 24.467574 D and the optimization energy is −3133.30494 hartree/particle; however, after the introduction of the epoxy group, the dipole moment decreases to 20.138302 D and the optimization energy becomes more negative at −3209.2595 hartree/particle. A similar pattern is observed when we further increase the number of carboxyl, hydroxy, and epoxy groups on the graphene sheet. Among all of the designed functionalized graphene structures, 322 having three carboxyl, two hydroxy, and two epoxy groups has the highest dipole moment of 30.312495 D and the one having three carboxyl, three hydroxy, and three epoxy groups shows the most negative optimization energy of −3697.686542 hartree/particle.

3.2. Molecular Electrostatic Potential (MEP). The MEP is a useful metric for determining the distribution of electrons in a molecule, which helps in identifying the positions that are susceptible to electrophilic and nucleophilic attacks.[37,38] To identify sites that are susceptible to nucleophilic and electrophilic attacks, MEP maps were created for graphene

https://doi.org/10.1021/acsomega.4c00173
ACS Omega 2024, 9, 16458−16468

and functionalized graphene (322), as shown in Figure 3. In the MEP representation, the red color indicates an area with

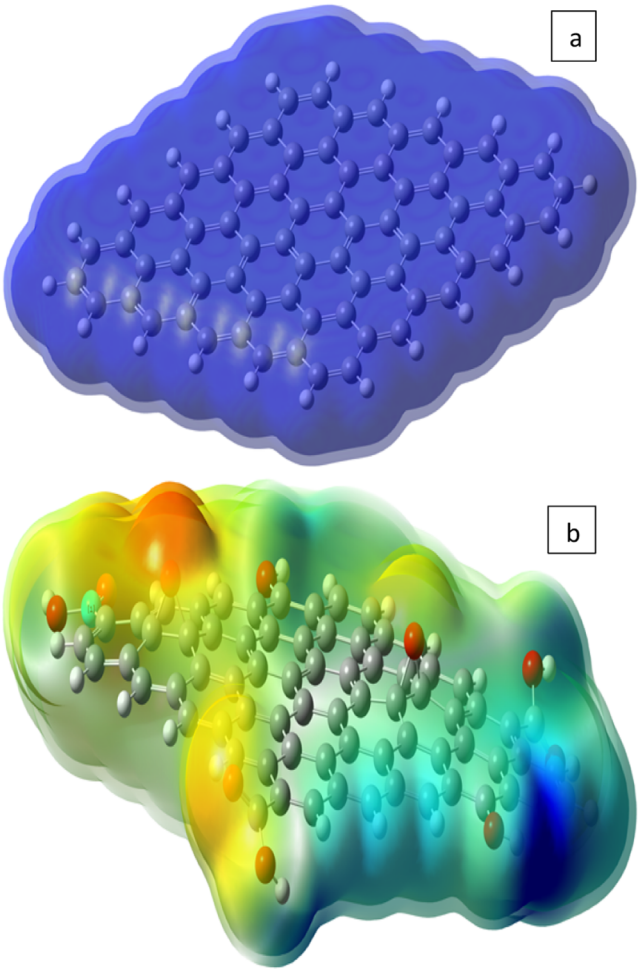

Figure 3. Molecular electrostatic potential diagram of (a) graphene and (b) 322.

increased electron density (negative), indicating it as the favored location for electrophilic attacks. In contrast, the presence of a blue color on the surface signifies a low electron concentration (positive), making it a favorable surface for nucleophilic attacks. The sequence of colors indicating electron density on the surface of the molecule is as follows blue < green < yellow < orange < red. This implies a higher propensity for strong adsorption on the 322 sheet compared to graphene.

3.3. Investigating the Information Obtained through Molecular Dynamics (MD) Simulations. The RMSF measures the degree of flexibility shown by individual atoms, indicating the extent of movement or fluctuation of a particular atom throughout a simulation. This approach also accounts for the conformational variations found in 322 during MD simulations. Furthermore, fluctuations in the average structure of 322 and graphene, measured in terms of the average atomic quadratic deviations. The RMSF analysis was performed for graphene and 322 in order to assess the displacement and stability of each atom during the simulation track. From Figure 4, it may be deduced that substantial changes in the structure of 322 in comparison to that of graphene occurred over the simulation time due to the presence of epoxy, hydroxy, and carboxyl groups. Figure 4 indicates that the molecule movements in the production phases of 322 indicate small oscillations with significant correlations, suggesting that the 322 is generally stable in a water-based solution

The RMSD is a quantitative metric that indicates the difference between two structures: a target structure and a reference structure. Within the realm of MD, our primary objective is to understand changes in the structures and their constituents throughout time in relation to their starting condition. The RMSD curve depicts the fluctuations in particle locations computed at different time points throughout the simulation period with respect to a fixed reference. The magnitude of the particle oscillations is directly proportional to the stability of the system. A less stable system would have more particle oscillations, which may be seen by a steeper slope in the RMSD curve. The RMSD value of graphene lies between 0.01 and 0.06 nm, whereas the 322 RMSD value ranges from 0.05 to 0.1 nm. A higher value of RMSD is obtained for 322 due to the presence of epoxy, hydroxy, and carboxyl groups on it. The RMSD value of both graphene and 322 lies in an acceptable range. Figure 5 illustrates the RMSD

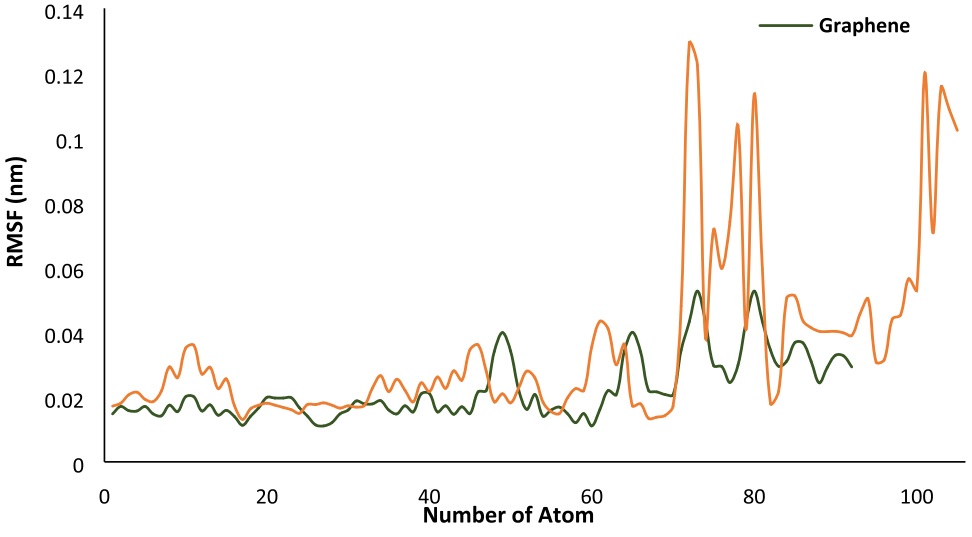

Figure 4. RMSF plot of 322 and graphene.

https://doi.org/10.1021/acsomega.4c00173
ACS Omega 2024, 9, 16458−16468

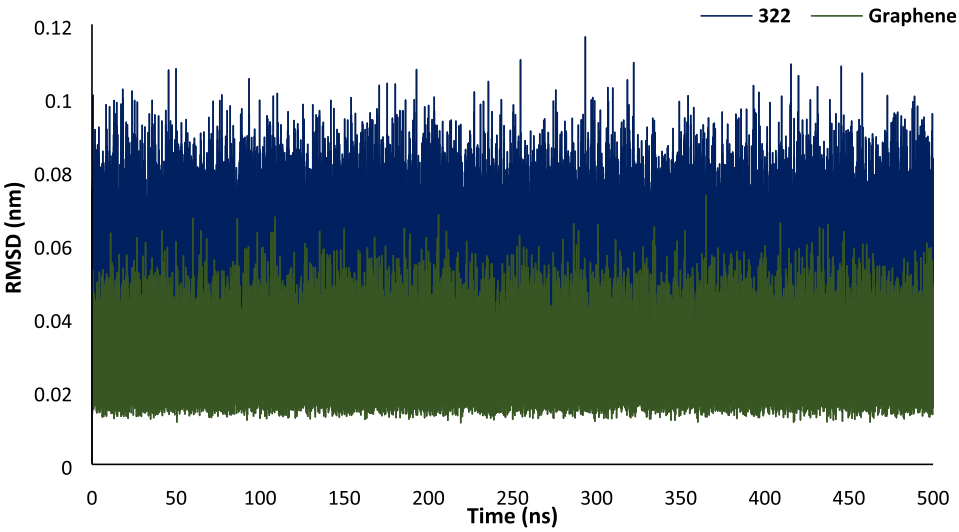

Figure 5. RMSD plot of 322 and graphene.

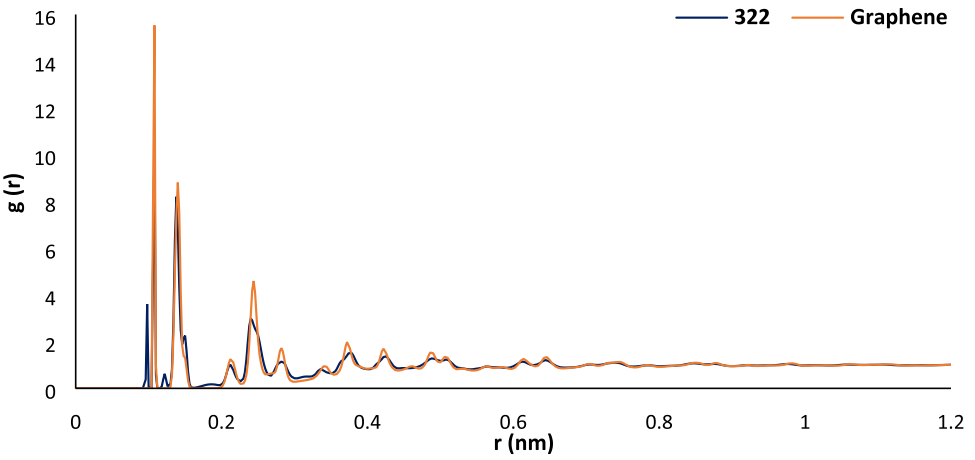

Figure 6. RDF plots of 322 and graphene in water.

of 322 and graphene, which shows minimal deviation over a time span of 500 ns.

The radial distribution function (RDF) provides useful information about the spatial distribution of particles in a system. In this work, the RDF was performed to reveal the structural properties of the system under consideration. The profile of the particle dispersion as it varies in distance from a reference particle is shown in Figure 6. The RDF plot of 322 and graphene displayed different peaks and troughs, indicating the presence of certain ordering and configurations inside the system. The prominent peaks in 322 correspond to the desired interparticle distances, implying the presence of well-defined coordination shells. Furthermore, RDF analysis of 322 and graphene was used to determine the nature of particle interactions in water. Identification of distinctive peaks corresponding to coordination shells reveals information regarding particle local ordering and packing, offering light on the underlying structural properties. The RDF plot gives information about the spatial organization of particles inside the system.

3.4. Natural Bond Orbital (NBO). NBO analysis of graphene and 322 was performed by using the NBO 6 module in Gaussian 16.0.[39] The NBO analysis is an effective approach for exploring both intra- and intermolecular bondings, as well as interactions among bonds. It provides a convenient framework for analyzing charge transfer and conjugative interactions within molecular systems.[40,37] This method gives detailed information about specific electron donor and acceptor orbitals, along with the interacting stabilization energy derived from the second-order perturbation theory. The magnitude of the E_2 value gives an idea about the strength of interaction between electron donors and acceptors. In simpler terms, a higher E_2 value indicates a more pronounced tendency for electron donation from donors to acceptors and a greater extent of conjugation throughout the entire molecular system. After the introduction of the functional group on graphene, the E_2 value increases between the donor and acceptor atoms where the functional group is present. Conjugation in 322 increased as compared to graphene due to the presence of epoxy, hydroxy, and carboxyl groups. The structures of 322 and graphene with atom numbers are shown in Figure 7. Details of the NBO of 322 and graphene are given in Tables S1 and S2.

4. CONCLUSIONS

In this work, the computational analysis of functionalized graphene electronic characteristics using DFT calculations has provided an important understanding of the behavior of

https://doi.org/10.1021/acsomega.4c00173
ACS Omega 2024, 9, 16458−16468

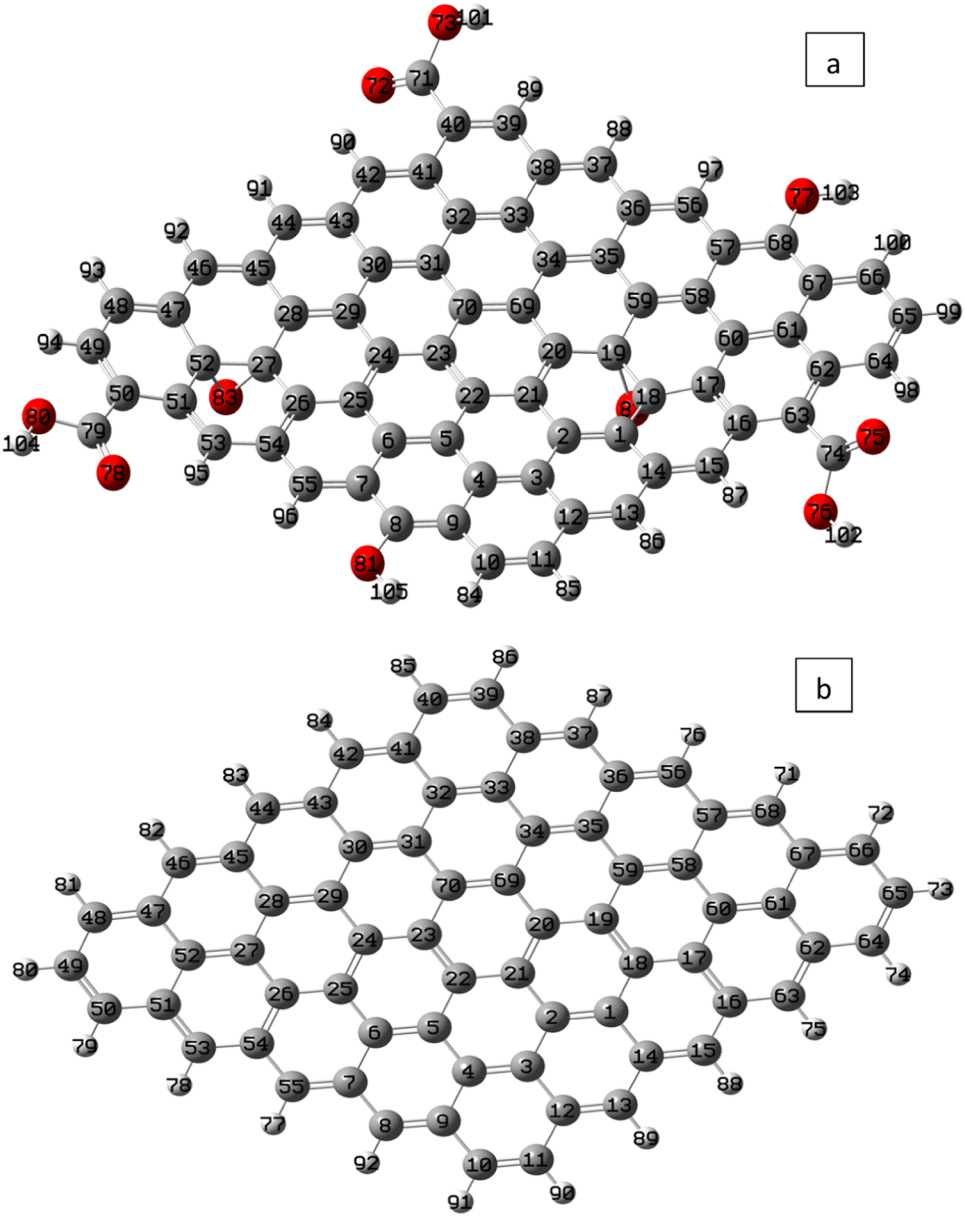

Figure 7. Representation of (a) 322 and (b) graphene with atom number.

graphene when the functional group and number are changed. The study revealed that the introduction of epoxy groups increased the energy gap ($E_{HOMO} - E_{LUMO}$) on a graphene sheet, signifying enhanced stability and reduced chemical reactivity. Conversely, the addition of carboxyl groups decreased the energy gap, indicating a heightened chemical reactivity. Hydroxy groups, when individually added, had negligible effects on the energy gap. Global chemical reactivity descriptors demonstrated that the incorporation of oxygen-containing functional groups generally led to more negative values of μ, reflecting increased stability. Interestingly, functionalized graphene structures with a combination of carboxyl, hydroxyl, and epoxy groups exhibited the highest electrophilicity index, suggesting a strong binding capacity. Among all of the designed functionalized graphene, 322 shows maximum polarity with a dipole moment of 30.312495 D. MEP maps highlighted the susceptibility of 322 to electrophilic attacks, especially with various functional groups, compared to graphene. MD simulations confirmed the stability of 322 over 500 ns, as evidenced by RMSD and small fluctuations in RMSF analyses provides a comprehensive understanding of the electronic properties and potential applications of 322.

■ ASSOCIATED CONTENT

Supporting Information

The Supporting Information is available free of charge at https://pubs.acs.org/doi/10.1021/acsomega.4c00173.

Natural bond orbital (NBO) analysis results are included, offering additional insights into the molecular interactions (Tables S1 and S2) (PDF)

■ AUTHOR INFORMATION

Corresponding Authors

Prashant Singh − *Department of Chemistry, Atma Ram Sanatan Dharma College, University of Delhi, Delhi 110021, India;* orcid.org/0000-0001-9648-2275; Email: psingh@arsd.du.ac.in

https://doi.org/10.1021/acsomega.4c00173
ACS Omega 2024, 9, 16458−16468

Oyirwoth P. Abedigamba − *Department of Physics, Kyambogo University, 1 Kampala, Uganda;* orcid.org/0000-0002-9755-9112; Email: oyigamba@kyu.ac.ug

Authors

Madhur Babu Singh − *Department of Chemistry, Atma Ram Sanatan Dharma College, University of Delhi, Delhi 110021, India; Department of Chemistry, SRM Institute of Science & Technology, NCR Campus, Ghaziabad 201204, India*

Pallavi Jain − *Department of Chemistry, SRM Institute of Science & Technology, NCR Campus, Ghaziabad 201204, India*

Faruq Mohammad − *Department of Chemistry, College of Science, King Saud University, Riyadh 11451, Kingdom of Saudi Arabia;* orcid.org/0000-0002-9318-9986

Indra Bahadur − *Department of Chemistry, Material Science, Innovation and Modelling (MaSIM) Research Focus Area, North-West University (Mafikeng Campus), Mmabatho 2735, South Africa*

Complete contact information is available at: https://pubs.acs.org/10.1021/acsomega.4c00173

Notes

The authors declare no competing financial interest.

■ ACKNOWLEDGMENTS

The authors are thankful to Professor B. Jayaram for utilizing the facilities of SCFBio, Indian Institute of Technology, Delhi, India. KSU author acknowledges the funding from Researchers Supporting Project number (RSP2024R355), King Saud University, Riyadh, Saudi Arabia.

■ REFERENCES

(1) Zhou, S.; Bongiorno, A. Density Functional Theory Modeling of Multilayer "Epitaxial" Graphene Oxide. *Acc. Chem. Res.* **2014**, *47* (11), 3331−3339.

(2) Gómez, E. V.; Guarnizo, N. A. R.; Perea, J. D.; López, A. S.; Prías-Barragán, J. J. Exploring Molecular and Electronic Property Predictions of Reduced Graphene Oxide Nanoflakes via Density Functional Theory. *ACS Omega* **2022**, *7* (5), 3872−3880, DOI: 10.1021/acsomega.1c00963.

(3) Xiang, Q.; Zhong, B.; Tan, H.; Navik, R.; Liu, Z.; Zhao, Y. Improved Dispersibility of Graphene in an Aqueous Solution by Reduced Graphene Oxide Surfactant: Experimental Verification and Density Functional Theory Calculation. *Langmuir* **2022**, *38* (27), 8222−8231.

(4) Sánchez-Cepeda, A.; Cedeño, E.; Marín, E.; Pazos, M. C.; Ingrid, S.-C.; de Jesús Muñoz, E.; Vera-Graziano, R. Evaluation of the Dispersion Properties of Graphene Oxide/Cetyltrimethylammonium Bromide for Application in Nanocomposite Materials. *RSC Adv.* **2024**, *14* (5), 3267−3279, DOI: 10.1039/D3RA04689C.

(5) Tabari, L.; Farmanzadeh, D. Yttrium Doped Graphene Oxide as a New Adsorbent for H2O, CO, and Ethylene Molecules: Dispersion-Corrected DFT Calculations. *Appl. Surf. Sci.* **2020**, *500*, No. 144029.

(6) Liu, W.; Speranza, G. Tuning the Oxygen Content of Reduced Graphene Oxide and Effects on Its Properties. *ACS Omega* **2021**, *6* (9), 6195−6205.

(7) Koo, D.; Sung, J.; Suh, H.; Bae, S.; So, H. Comprehensive Analysis of CNT/NS/GO Composites: Dispersion Effect of Graphene Oxide for Environmental Sensor Application. *Composites, Part A* **2023**, *173*, No. 107639.

(8) Rosas, J. J. H.; Ramírez Gutiérrez, R. E.; Escobedo-Morales, A.; Anota, E. C. First Principles Calculations of the Electronic and Chemical Properties of Graphene, Graphane, and Graphene Oxide. *J. Mol. Model.* **2011**, *17*, 1133−1139, DOI: 10.1007/s00894-010-0818-1.

(9) Ray, S. C.Application and Uses of Graphene Oxide and Reduced Graphene Oxide. In *Applications of Graphene and Graphene-Oxide Based Nanomaterials*; Elsevier, 2015; Chapter 2, Vol. *6*, pp 39−55.

(10) Hashemzadeh, H.; Raissi, H. Understanding Loading, Diffusion and Releasing of Doxorubicin and Paclitaxel Dual Delivery in Graphene and Graphene Oxide Carriers as Highly Efficient Drug Delivery Systems. *Appl. Surf. Sci.* **2020**, *500*, No. 144220.

(11) Liu, C.; Luo, X. Potential Molecular and Graphene Oxide Chelators to Dissolve Amyloid-β Plaques in Alzheimer's Disease: A Density Functional Theory Study. *J. Mater. Chem. B* **2021**, *9* (11), 2736−2746.

(12) Das, P.; Rout, B.; Manju, U.; Chatterjee, S. Tunable Wettability and Conductivity of the Graphene Oxide Surface with Insights from Density Functional Theory and Molecular Dynamics Investigations. *J. Phys. Chem. C* **2020**, *124* (19), 10541−10549.

(13) Jafari, Z.; Baharfar, R.; Rad, A. S.; Asghari, S. Potential of Graphene Oxide as a Drug Delivery System for Sumatriptan: A Detailed Density Functional Theory Study. *J. Biomol. Struct. Dyn.* **2021**, *39* (5), 1611−1620.

(14) Khine, Y. Y.; Wen, X.; Jin, X.; Foller, T.; Joshi, R. Functional Groups in Graphene Oxide. *Phys. Chem. Chem. Phys.* **2022**, *24* (43), 26337−26355.

(15) Keramatinia, M.; Ramezanzadeh, B.; Mahdavian, M.; Bahlakeh, G. Chemically Controlled Nitrogen-Doped Reduced-Graphene/Graphite Oxide Frameworks for Aiding Superior Thermal/Anti-Corrosion Performance: Integrated DFT-D & Experimental Evaluations. *Chem. Eng. J.* **2022**, *437*, No. 135241, DOI: 10.1016/j.cej.2022.135241.

(16) Kumari, K.; Singh, M. B.; Tomar, N.; Kumar, A.; Kumar, V.; Dabodhia, K. L.; Singh, P. Adsorption of Pesticides Using Graphene Oxide through Computational and Experimental Approach. *J. Mol. Struct.* **2023**, *1291*, No. 136043, DOI: 10.1016/j.molstruc.2023.136043.

(17) Akintemi, E. O.; Govender, K. K.; Singh, T. A DFT Study of the Chemical Reactivity Properties, Spectroscopy and Bioactivity Scores of Bioactive Flavonols. *Comput. Theor. Chem.* **2022**, *1210*, No. 113658.

(18) Mehmeti, V.; Halili, J.; Berisha, A. Which Is Better for Lindane Pesticide Adsorption, Graphene or Graphene Oxide? An Experimental and DFT Study. *J. Mol. Liq.* **2022**, *347*, No. 118345.

(19) Zhang, Y.; Zhao, Y.; Yang, Y.; Liu, P.; Liu, J.; Zhang, J. DFT Study on Hg0 Adsorption over Graphene Oxide Decorated by Transition Metals (Zn, Cu and Ni). *Appl. Surf. Sci.* **2020**, *525*, No. 146519.

(20) Lv, S.; Liu, D.; Sun, Y.; Li, M.; Zhou, Y.; Song, C.; Wang, D. Graphene Oxide Coupled High-Index Facets CdZnS with Rich Sulfur Vacancies for Synergistic Boosting Visible-Light-Catalytic Hydrogen Evolution in Natural Seawater: Experimental and DFT Study. *J. Colloid Interface Sci.* **2022**, *623*, 34−43.

(21) Li, Z.; Wan, H.; Shi, Y.; Ouyang, P. Personal Experience with Four Kinds of Chemical Structure Drawing Software: Review on ChemDraw, ChemWindow, ISIS/Draw, and ChemSketch. *J. Chem. Inf. Comput. Sci.* **2004**, *44* (5), 1886−1890.

(22) Frisch, M. J.; Trucks, G. W.; Schlegel, H. B.; Scuseria, G. E.; Robb, M. A.; Cheeseman, J. R.; Scalmani, G.; Barone, V.; Petersson, G. A.; Nakatsuji, H.; Li, X.; Caricato, M.; Marenich, A. V.; Bloino, J.; Janesko, B. G.; Gomperts, R.; Mennucci, B.; Hratchian, H. P.; Ortiz, J. V.; Izmaylov, A. F.; Sonnenberg, J. L.; Williams-Young, D.; Ding, F.; Lipparini, F.; Egidi, F.; Goings, J.; Peng, B.; Petrone, A.; Henderson, T.; Ranasinghe, D.; Zakrzewski, V. G.; Gao, J.; Rega, N.; Zheng, G.; Liang, W.; Hada, M.; Ehara, M.; Toyota, K.; Fukuda, R.; Hasegawa, J.; Ishida, M.; Nakajima, T.; Honda, Y.; Kitao, O.; Nakai, H.; Vreven, T.; Throssell, K.; Montgomery, J. A., Jr; Peralta, J. E.; Ogliaro, F.; Bearpark, M. J.; Heyd, J. J.; Brothers, E. N.; Kudin, K. N.; Staroverov, V. N.; Keith, T. A.; Kobayashi, R.; Normand, J.; Raghavachari, K.; Rendell, A. P.; Burant, J. C.; Iyengar, S. S.; Tomasi, J.; Cossi, M.; Millam, J. M.; Klene, M.; Adamo, C.; Cammi, R.; Ochterski, J. W.; Martin, R. L.; Morokuma, K.; Farkas, O.; Foresman, J. B.; Fox, D. J. *Gaussian 16, Rev. C. 01*; Gaussian Inc., 2016.

(23) Dennington, R.; Keith, T. A.; Millam, J. M. *GaussView 6.0. 16.*; Semichem Inc.: Shawnee Mission, KS, USA, 2016.
(24) Baboul, A. G.; Curtiss, L. A.; Redfern, P. C.; Raghavachari, K. Gaussian-3 Theory Using Density Functional Geometries and Zero-Point Energies. *J. Chem. Phys.* **1999**, *110* (16), 7650−7657.
(25) Andzelm, J.; Wimmer, E. Density Functional Gaussian-Type-Orbital Approach to Molecular Geometries, Vibrations, and Reaction Energies. *J. Chem. Phys.* **1992**, *96* (2), 1280−1303.
(26) Andersson, M. P.; Uvdal, P. New Scale Factors for Harmonic Vibrational Frequencies Using the B3LYP Density Functional Method with the Triple-ζ Basis Set 6-311 + G (d, P). *J. Phys. Chem. A* **2005**, *109* (12), 2937−2941.
(27) Singh, M. B.; Kumari, K.; Aslam, M.; Vishvakarma, V. K.; Bahadur, I.; Singh, P. Role of Alkyl Chain Present in the Cations of Ionic Liquids on Stabilization of Silver Nanoparticle: DFT and TD-DFT Studies. *J. Mol. Liq.* **2023**, No. 122168, DOI: 10.1016/j.molliq.2023.122168.
(28) Bauschlicher, C. W., Jr; Partridge, H. A Modification of the Gaussian-2 Approach Using Density Functional Theory. *J. Chem. Phys.* **1995**, *103* (5), 1788−1791.
(29) Van Der Spoel, D.; Lindahl, E.; Hess, B.; Groenhof, G.; Mark, A. E.; Berendsen, H. J. C. GROMACS: Fast, Flexible, and Free. *J. Comput. Chem.* **2005**, *26* (16), 1701−1718.
(30) Huang, J.; MacKerell, A. D., Jr. CHARMM36 All-atom Additive Protein Force Field: Validation Based on Comparison to NMR Data. *J. Comput. Chem.* **2013**, *34* (25), 2135−2145.
(31) Mark, P.; Nilsson, L. Structure and Dynamics of the TIP3P, SPC, and SPC/E Water Models at 298 K. *J. Phys. Chem. A* **2001**, *105* (43), 9954−9960.
(32) James, F. Monte Carlo Theory and Practice. *Rep. Prog. Phys.* **1980**, *43* (9), 1145.
(33) Singh, M. B.; Prajapat, A.; Jain, P.; Singh, P.; Bahadur, I.; Kaushik, N. K.; Kaushik, N.; Kumari, K. Investigate the Ability of Deep Eutectic Solvent (ChCl-Glycerol) to Sense the Sulphur Dioxide Using Density Functional Theory Calculations and Molecular Dynamics Simulations. *J. Mol. Liq.* **2023**, *388*, No. 122720, DOI: 10.1016/j.molliq.2023.122720.
(34) Petersen, H. G. Accuracy and Efficiency of the Particle Mesh Ewald Method. *J. Chem. Phys.* **1995**, *103* (9), 3668−3679.
(35) McGibbon, R. T.; Beauchamp, K. A.; Harrigan, M. P.; Klein, C.; Swails, J. M.; Hernández, C. X.; Schwantes, C. R.; Wang, L.-P.; Lane, T. J.; Pande, V. S. MDTraj: A Modern Open Library for the Analysis of Molecular Dynamics Trajectories. *Biophys. J.* **2015**, *109* (8), 1528−1532.
(36) Hasanzade, Z.; Raissi, H. Assessment of the Chitosan-Functionalized Graphene Oxide as a Carrier for Loading Thioguanine, an Antitumor Drug and Effect of Urea on Adsorption Process: Combination of DFT Computational and Molecular Dynamics Simulation Studies. *J. Biomol. Struct. Dyn.* **2019**, *37* (10), 2487−2497.
(37) Ramalingam, S.; Karabacak, M.; Periandy, S.; Puviarasan, N.; Tanuja, D. Spectroscopic (Infrared, Raman, UV and NMR) Analysis, Gaussian Hybrid Computational Investigation (MEP Maps/HOMO and LUMO) on Cyclohexanone Oxime. *Spectrochim. Acta, Part A* **2012**, *96*, 207−220.
(38) Abdel-Bary, A. S.; Tolan, D. A.; Nassar, M. Y.; Taketsugu, T.; El-Nahas, A. M. Chitosan, Magnetite, Silicon Dioxide, and Graphene Oxide Nanocomposites: Synthesis, Characterization, Efficiency as Cisplatin Drug Delivery, and DFT Calculations. *Int. J. Biol. Macromol.* **2020**, *154*, 621−633.
(39) Glendening, E. D.; Landis, C. R.; Weinhold, F. NBO 6.0: Natural Bond Orbital Analysis Program. *J. Comput. Chem.* **2013**, *34* (16), 1429−1437.
(40) Weinhold, F.; Landis, C. R.; Glendening, E. D. What Is NBO Analysis and How Is It Useful? *Int. Rev. Phys. Chem.* **2016**, *35* (3), 399−440.

https://doi.org/10.1021/acsomega.4c00173
ACS Omega 2024, 9, 16458−16468